



Novel visible-light-sensitized Chl-Mg/P25 catalysts for photocatalytic degradation of rhodamine B

Thanaree Phongamwong^{a,b}, Waleeporn Donphai^{a,b}, Phatthanon Prasitchoke^c, Christoph Rameshan^d, Noelia Barrabeís^d, Wantana Klysubun^e, Günther Rupprechter^d, Metta Chareonpanich^{a,b,*}

^a KU-Green Catalysts Group, Department of Chemical Engineering, Faculty of Engineering, Kasetsart University, Bangkok 10900, Thailand

^b NANOTEC Center for Nanoscale Materials Design for Green Nanotechnology and Center for Advanced Studies in Nanotechnology for Chemical, Food and Agricultural Industries, KU Institute for Advanced Studies, Kasetsart University, Bangkok 10900, Thailand

^c PTT Global Chemical Public Company Limited, Bangkok 10900, Thailand

^d Institute of Materials Chemistry, Technische Universität Wien, Getreidemarkt 9/BC/01, Vienna 1060, Austria

^e Synchrotron Light Research Institute, Nakhon Ratchasima 30000, Thailand

ARTICLE INFO

Article history:

Received 26 December 2016

Received in revised form 10 February 2017

Accepted 11 February 2017

Available online 14 February 2017

Keywords:

Chlorophyll

Mg/P25

Spirulina

RhB degradation

Visible light

ABSTRACT

Photocatalytic reaction is known as one of the most promising processes to reduce global warming and environmental problems as well as offer sustainable energy sources. As nano-bio hybrid materials are potential alternatives for improving the efficiency of photocatalytic reactions, a unique chlorophyll and Mg co-modified P25 (Degussa P25, which consists of mixed phases between anatase and rutile) catalyst was synthesized and used as a visible light reactive photocatalyst in this research. The activity of obtained catalysts was evaluated from photocatalytic degradation of rhodamine B (RhB) under visible light, and the effect of chlorophyll source, co-modified chlorophyll and magnesium, and their loading amounts on photodegradation of RhB were investigated. It was found that the loading of extracted chlorophyll gave higher activity than that of *Spirulina* due to its greater possibility for direct contact between chlorophyll and P25, leading to more efficient electron transfer from chlorophyll to P25. In addition, loading free Mg together with chlorophyll led to the formation of a new complex structure, resulting in synergistic effect between chlorophyll-Mg and P25, and therefore an increase in photocatalytic performance and good reusability of catalysts. Proper amounts of chlorophyll and Mg loading on P25 (0.5Chl-0.1Mg/P25) could promote the photocatalytic activities such that they are approximately 2.3, 1.3 and 2.1 times those of P25, 0.5Chl/P25 and 0.1Mg/P25, respectively.

© 2017 Elsevier B.V. All rights reserved.

1. Introduction

In recent years, the world energy crisis and environmental pollution, including water and air contamination, have become main issues in the lives of humans [1,2]. Efficient utilization of solar energy, one of the cleanest and largest renewable energy sources available, can potentially help lessen the above-mentioned problems. Photocatalytic reaction, as an eco-friendly alternative process, has received widespread attention as it is proven to be an efficient and economical approach. This photoreaction can make

use of solar energy to simultaneously reduce the environmental problems by offering alternative and sustainable chemical feedstock, as well as green energy [3–5].

Titanium dioxide (TiO_2) is the most investigated semiconductor photocatalyst due to its availability, environmentally friendliness, and high chemical stability [6–8]. Due to these remarkable properties, TiO_2 has been widely used in various fields of photocatalytic application, especially environmental and energy-related purposes (e.g., degradation of pollutants [9,10], CO_2 reduction [11], and water splitting [4]). It is well known that the crystalline structure and electronic band structure of TiO_2 have significant influences on photocatalytic performance of TiO_2 . Among the stable phases of TiO_2 , rutile is the most chemically stable phase with high photo-oxidation activity for oxygen evolution [12,13], while anatase has a higher activity in photo-decomposition of organic molecules [14,15]. More interestingly, the mixed phases between anatase and

* Corresponding author at: KU-Green Catalysts Group, Department of Chemical Engineering, Faculty of Engineering, Kasetsart University, Bangkok 10900, Thailand.

E-mail addresses: fengmtc@ku.ac.th, iamannmetta@gmail.com
(M. Chareonpanich).

rutile, such as Degussa P25, have been found to exhibit higher photocatalytic activity for a wide range of reactions relative to their single phases [16–18]. The synergetic effect between band alignment of anatase and rutile helps lower the effective band gap and enhances the photoexcited charge separation between the two phases, resulting in improved photocatalytic performance [19,20].

TiO_2 photocatalysis, however, has major drawbacks in the rapid recombination of photo-induced electron-hole ($e^- - h^+$) pairs, low quantum yield, and low efficiency in the visible light region because of its wide band gap energy (ca. 3.2 eV for anatase and 3.0 eV for rutile) [21–24]. In order to overcome such disadvantages of TiO_2 catalyst, many intense efforts have been made to improve its photocatalytic efficiency by modifying either structures [25–27] or compositions [28–31]. Among various novel compounds that have been developed, nano-bio hybrid materials with natural photosensitizer characteristics are one of the potential alternatives to enhance the photocatalytic activity. In natural photosynthesis of plants and algae, chlorophyll *a*, which is a major photosynthetic pigment, plays an important role in solar energy absorption in the range of red and blue light to produce sources of energy [32–34]. With the intention of utilizing and imitating effective processes from nature and bearing in mind the role that chlorophyll can play, the combination of TiO_2 nanoparticles and chlorophyll molecules to produce novel and unique photocatalysts has been explored [35–39].

Our previous research [40] reported the activity of *Spirulina*-modified N- TiO_2 catalyst (Sp/N- TiO_2) in CO_2 photoreduction for the first time. *Spirulina platensis* was selected to be the chlorophyll source and was used to modify the photocatalyst due to its high chlorophyll content (approximately 1.15% of its biomass) and photosynthesis rate, as well as ease of cultivation [41,42]. Comparing to the undoped TiO_2 and N- TiO_2 catalysts, Sp/N- TiO_2 exhibited notable enhancements in CO_2 photoreduction under visible-light irradiation. The chlorophyll in *Spirulina* presumably acted as a sensitizer and gave additional electrons to the catalyst. These electrons donated from chlorophyll in *Spirulina* directly improved the photocatalytic efficiency as well as the stability of photocatalyst to some extent. However, the activities of the catalysts decreased when the percentage of chlorophyll in *Spirulina* was higher than a certain level, a fact which is possibly due to the formation of recombination centers of electron and hole.

The other important photocatalytic improvement strategy is to incorporate metals (i.e., Au, Ag, Pt, Ni, Cu, Mg) on TiO_2 to retard recombination of electron-hole pairs [9,43–45]. Of all metals, the utilization of Mg, which is the only metal in chlorophyll structure ($\text{C}_{55}\text{H}_{72}\text{O}_5\text{N}_4\text{Mg}$) and a key compound in natural photosynthesis, has a promising potential not only in enhancing photocatalytic efficiency [46–48], but also in improving catalyst stability by preventing chlorophyll degradation.

Owing to the unclarified evidence regarding the improvement of photocatalytic behavior in the presence of *Spirulina*, experiments on extracted chlorophyll-modified photocatalyst are therefore essential to identify the crucial factors affecting the performance of modified photocatalysts. Moreover, further investigation is still required not only to maximize the photocatalytic activity but also to improve catalyst stability. In this present study chlorophyll-Mg co-modified P25 (Chl-Mg/P25) photocatalysts were prepared and tested for their photocatalytic performances and stability in the degradation of rhodamine B (RhB) dye molecules under visible light. The source of chlorophyll and its loading amount have been investigated. It was found that the photocatalytic activity of Chl-Mg/P25 catalyst was remarkably enhanced due to its superior harvesting of visible light, high capacity of dye adsorption, and effective suppression of charge recombination.

2. Experimental

2.1. Catalysts preparation

2.1.1. Chlorophyll extraction

Dried *Spirulina* was incubated with a certain amount of methanol in a water bath at 70 °C for 2 min and then centrifuged at 3500 rpm for 5 min. The chlorophyll solution was collected from a clear supernatant solution. Finally, the amount of chlorophyll can be calculated from Eq. (1) [49]:

$$\text{Chlorophyll} = 13.9A_{665} 13.9A_{665} (\text{mg L}^{-1}) \quad (1)$$

where A_{665} is absorbance at 665 nm measured by a UV-vis spectrophotometer (Thermo Scientific, Genesys 10 series).

2.1.2. Loading of magnesium onto P25 catalyst

The Mg-loaded P25 catalysts were prepared by incipient wetness impregnation method. A certain amount of magnesium nitrate ($\text{Mg}(\text{NO}_3)_2 \cdot 6\text{H}_2\text{O}$: PanReac AppliChem, 98% purity) used as a Mg precursor was dissolved in deionized water and dropped onto commercial Degussa P25 (TiO_2 : Aldrich). The obtained mixture was then vigorously stirred for 1 h. After that, the mixture was dried by using a microwave oven at 800 W for 2 min. In this study, magnesium concentrations in the catalyst were 0.01, 0.1 and 0.2 wt.% Mg.

2.1.3. Preparation of chlorophyll or *Spirulina*-modified P25 and Mg/P25 catalysts

P25 and Mg/P25 catalysts were modified by using chlorophyll or *Spirulina* via incipient wetness impregnation method. Firstly, chlorophyll solution was added onto P25 and Mg/P25 catalysts, and then the mixture was continuously stirred at 40 °C overnight until the solvent was completely evaporated. The obtained catalysts were labeled as xChl-yMg/P25, where x and y are weight percentages of chlorophyll *a* and magnesium, respectively. In order to investigate the effect due to the chlorophyll source, *Spirulina*-modified P25 catalyst was prepared following the same procedure as described above. *Spirulina* solution obtained by dissolving powder of dried *Spirulina* in deionized water was used instead of chlorophyll solution. The loading amount of *Spirulina* was based on the amount of chlorophyll *a* in *Spirulina*. The obtained catalyst was labeled as zSp/P25, where z is weight percentage of chlorophyll *a* in *Spirulina*.

2.2. Catalyst characterization

The crystal structure of catalysts was examined by an X-ray diffractometer (Bruker D8 Advance) operated with monochromated Cu-K α radiation at room temperature. The crystallite sizes of catalysts were analyzed from X-ray diffraction (XRD) patterns using the Scherrer equation.

Nitrogen sorption isotherms of catalysts were examined at –196 °C using a Quantachrome Autosorp-1C instrument. The specific surface area of catalysts was obtained by using the Brunauer–Emmett–Teller (BET) analysis, and pore size distribution was calculated by using the Barrett–Joyner–Halenda (BJH) method. Specific pore volume was measured at a relative pressure of 0.995.

Morphology was analyzed and chemical element mapping of catalysts was performed by using field emission scanning electron microscopy (FE-SEM: JEOL, JSM-7600F) with energy dispersive X-ray spectroscopy (EDS: OXFORD, X-Max^N) operated at 15 keV with Pt-coating of the samples.

Fourier transform infrared spectroscopy, using equipment (FT-IR: Bruker TENSOR 27) with a DTGS detector, was performed in

the range of 4000–400 cm⁻¹ to examine functional groups of the catalysts.

Absorption spectra of catalysts were recorded with UV-vis diffuse reflectance spectroscopy (UV-vis DRS: JASCO, V-670) using BaSO₄ as a reflectance standard. The Kubelka–Munk function ($F(R)$), as shown in Eq. (2), and Tauc plots were used to determine band gap energies of the catalysts:

$$F(R) = (1 - R)^2 / 2R \quad (2)$$

where R is absolute reflectance of the catalyst layer.

X-ray photoelectron spectroscopy (XPS), comprised of a commercial UHV system with a Phoibos 100 hemispherical analyzer and a XR 50 X-ray source (all SPECS GmbH), was used to measure chemical states and surface atomic concentrations of the catalysts. Quantitative measurement of Ti 2p, O 1s, C 1s, N 1s, and Mg 2s was taken with a resolution of 0.1 eV per step. The commercial software package CasaXPS was used for background subtraction (Shirley), fitting, and quantitative chemical analysis. To calibrate the binding energy scale, the valence band spectra were used.

The electronic state and band structure of Mg in catalysts were examined by using X-ray absorption near edge structure (XANES) at Beamline 8 of the Synchrotron Light Research Institute (SLRI), Thailand. A double crystal Beryl (1010) monochromator was used for photon energy selection. Mg K-edge spectra were recorded at room temperature in fluorescence mode, and magnesium foil was used for calibration at an E_0 of 1303 eV. Three $\mu(E)$ data scans (~4 h per scan) were merged into one data file to improve the signal-to-noise ratio, and the obtained spectra were processed and analyzed using the Athena program.

The charge transfer process of catalysts was analyzed by using photoluminescence spectroscopy (PL: AvaSpec-2048TEC, Avantes) carried out at room temperature in the range of 300–700 nm using an excitation wavelength of 255 nm.

Inductively coupled plasma-optical emission spectrometry (ICP-OES: Agilent technologies 715) was performed to analyze the amount of magnesium in fresh and used 0.5Chl-0.1Mg/P25 catalysts.

2.3. Photocatalytic degradation measurements

In this research, a basic dye, rhodamine B ($C_{28}H_{31}ClN_2O_3$; HIME-DIA, practical grade), was used as a probe molecule to evaluate photocatalytic activities of the catalysts. For all experiments, the photocatalyst (30 mg) was suspended in 30 ml of RhB solution (30 or 60 mg/L) in a glass tube reactor by using a magnetic stirrer. Prior to the irradiation process, oxygen gas was introduced into the suspension under dark condition for 30 min to obtain the adsorption–desorption equilibrium. At equilibration, the concentration of RhB was measured and used as an initial concentration (C_0). Two 50 W LED floodlights (NULITE) located at each side of the reactor were used as the visible light sources to perform the photocatalytic reaction at room temperature. The average light intensity at the reaction zone was approximately $5.86 \pm 0.04 \text{ mW cm}^{-2}$. During photodegradation, the samples were taken from the reactor at certain time intervals and centrifuged to separate photocatalyst particles from the solution. The residual concentration of RhB was measured at a wavelength of 554 nm using a UV-vis spectrophotometer (Thermo Scientific, Genesys 10 series). In order to study the effects of photocatalysts on RhB degradation, a blank experiment with the absence of photocatalyst was also performed as a direct photolysis.

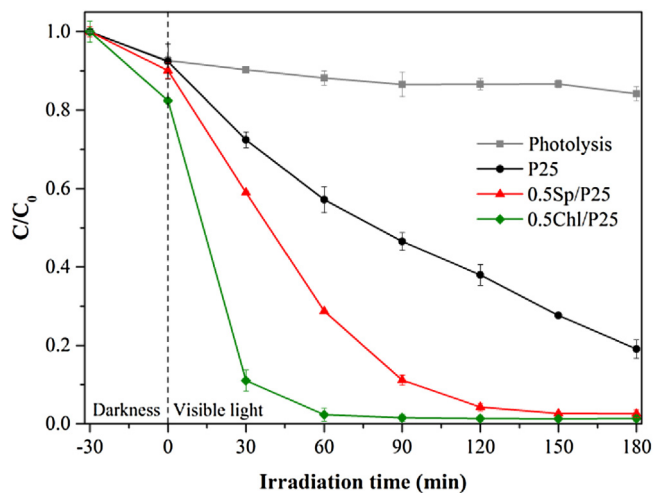


Fig. 1. Photocatalytic degradation of rhodamine B over P25 and modified P25 catalysts (RhB = 30 mg/L).

Table 1

Pseudo-first-order kinetic rate constant (k), regression coefficient (R^2), and percentage degradation of RhB under visible-light irradiation.

Catalysts	RhB concentration (mg/L)	$k (10^{-3} \text{ min}^{-1})$	R^2	Degradation ^a (%)
None	30	0.55 ± 0.04	0.840	9.15
P25	30	8.05 ± 0.23	0.986	78.62
	60	6.93 ± 0.19	0.984	33.60
0.5Sp/P25	30	23.53 ± 0.91	0.979	97.17
	60	3.65 ± 0.14	0.977	21.28
0.5Chl/P25	30	60.80 ± 2.21	0.993	98.38
	60	15.90 ± 0.61	0.976	63.75
	60	14.67 ± 0.32	0.991	60.67
	60	7.76 ± 0.20	0.986	36.36
	60	19.84 ± 1.44	0.928	74.89
	60	22.00 ± 1.20	0.956	76.77
0.5Chl-0.2Mg/P25	60	16.60 ± 1.20	0.927	68.07

^a Irradiation time for RhB concentration as 30 mg/L and 60 mg/L are 3 h and 1 h, respectively.

3. Results and discussion

3.1. Outstanding performance of chlorophyll-modified P25 catalysts

In this present work, the chlorophyll-modified P25 catalysts were examined for their adsorption and visible-light-driven photocatalytic degradation activities of RhB dye (30 mg/L), in comparison with P25 catalyst. As shown in Fig. 1 and Table 1, the degradation efficiency of photolysis (i.e., without catalyst) was approximately 9% in 3 h under visible-light illumination. The dye adsorption and degradation efficiencies were remarkably increased when P25 and modified P25 catalysts were applied following the order of: P25 < 0.5Sp/P25 < 0.5Chl/P25. These results indicated that both chlorophyll sources could enhance the photocatalytic performance of P25; however, the one with extracted chlorophyll loading exhibited a greater activity than that of *Spirulina* loading.

The effect of chlorophyll amounts on photocatalytic performance was also examined and is reported in Fig. 2A. For clearer observation of photocatalytic activity, the concentration of RhB in this series of experiments was increased from 30 to 60 mg/L. As shown in Fig. 2A, there was significantly more enhancement in dye adsorption in all Chl/P25 catalysts compared to P25 catalyst. The photodegradation efficiency of RhB increased with increasing amount of chlorophyll loading. However, the loading amount

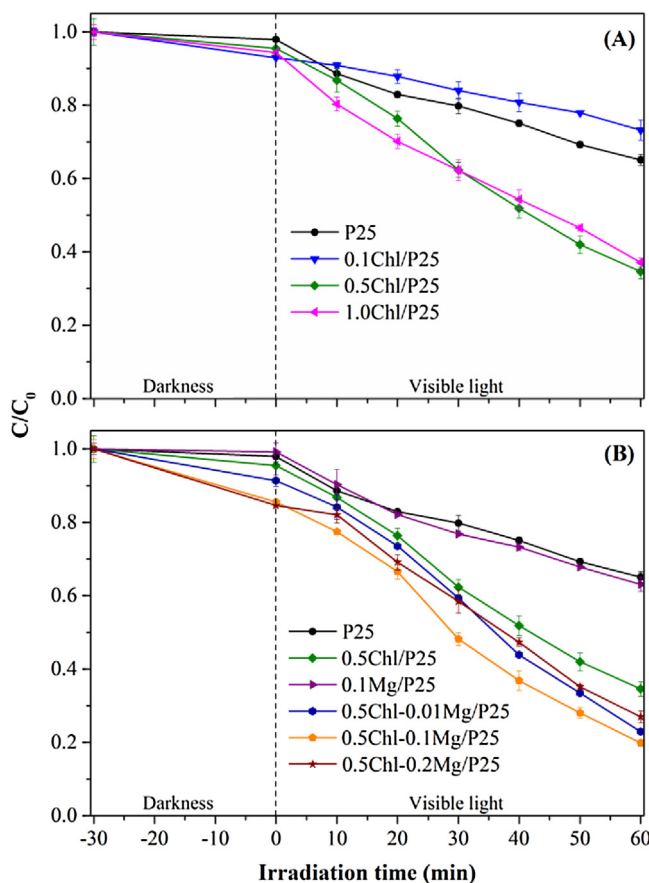


Fig. 2. Photocatalytic degradation of rhodamine B over P25 and modified P25 catalysts (RhB = 60 mg/L).

of more than 0.5 wt.% led to a slight decrease in the degradation activity (from ~64% to ~61% in 1 h) under illumination (Table 1).

The effects of magnesium and its loading amount on photocatalytic performance of optimal Chl/P25 catalyst were further examined, and the results are shown in Fig. 2B. Without the presence of chlorophyll, dye adsorption over P25 modified with 0.1 wt.% Mg was 2.4 times lower than that over the P25 catalyst. Interestingly, the addition of Mg on chlorophyll-modified catalyst (0.5Chl/P25) could obviously increase the adsorption of RhB dye. The dye adsorption efficiencies over 0.5Chl/P25 catalysts with 0.01, 0.1, and 0.2 wt.% Mg were, respectively approximately 1.9, 3.2, and 3.4 times higher than that of the 0.5Chl/P25 catalyst.

In terms of photocatalytic activity, the use of both Mg and chlorophyll loaded on P25 catalyst notably enhanced the dye degradation efficiency. The photoactivity of Chl-Mg/P25 catalysts was in the following order of: 0.5Chl-0.2Mg/P25 < 0.5Chl-0.01Mg/P25 < 0.5Chl-0.1Mg/P25. The 0.5Chl-0.1Mg/P25 catalyst showed a RhB adsorption of ~14% in dark condition and exhibited a photodegradation efficiency of approximately ~77% under visible light illumination for 1 h (Table 1). These results indicated that both chlorophyll and magnesium, as well as their amounts, play crucial roles in dye adsorption and visible-light-driven photocatalytic activity of the catalysts. From Fig. 2 and Table 1, it can be seen that the photocatalytic degradation of co-modified 0.5Chl-0.1Mg/P25, single-modified 0.5Chl/P25, and 0.1Mg/P25 were approximately 43%, 30%, and 3% higher than that of P25 catalyst, respectively. These results clearly confirmed the synergistic effect between chlorophyll and magnesium co-modified on P25 catalyst, an effect which is responsible for the elevation in photocatalytic activity. The amount of CO₂ produced from photodegradation of RhB

over 0.5Chl-0.1Mg/P25 catalyst was also analyzed by using a gas chromatograph (Shimadzu GC-2014 equipped with a thermal conductivity detector (TCD)). As shown in Fig. S1, the amount of produced CO₂ was found to gradually increase through a reaction time period of 90 min, which indicated the complete mineralization of RhB dye to CO₂ product.

The kinetics of RhB degradation over modified P25 catalysts were calculated using a pseudo-first-order kinetic model [50–52], as described by the following equation:

$$\ln(C_0/C) = kt \quad (3)$$

where C₀ and C (mg/L) are the RhB concentration at initial time (t=0) and time t, respectively; k (min⁻¹) is an apparent pseudo-first-order kinetic rate constant; and t (min) is irradiation time. The k value was calculated from linear regression of slope of the plot between ln(C₀/C) and irradiation time (see Fig. S2). The high regression coefficients (R²) of the kinetic plots reported in Table 1 evidently indicated the good agreement between these pseudo-first-order kinetics of RhB photocatalytic degradation and previous studies [53,54].

As can be seen in Table 1, the degradation rate (that is, the kinetic rate constant k) was found to remarkably increase through the introduction of P25 catalysts. With a RhB concentration of 60 mg/L, the highest degradation rate was achieved using 0.5Chl-0.1Mg/P25 catalyst (22.00×10^{-3} min⁻¹)—a rate which was approximately 3.2, 1.4, and 2.8 times higher than that of un-modified P25, single-modified 0.5Chl/P25, and 0.1Mg/P25 catalysts, respectively. In addition, when increasing the initial RhB concentrations from 30 to 60 mg/L, the percentage degradation and degradation rate over P25 and modified P25 catalysts decreased. This was due to the reduction of incident photon flux from the visible-light sources, resulting from the increase of initial RhB concentration and leading to fewer active sites on the photocatalyst surface [51,55].

3.2. Effects of crystal structure, morphology and surface characteristics of modified P25 catalysts on photocatalytic activities

Considering the physical structure of catalysts, it can be seen that the characteristic peaks of XRD patterns shown in Fig. S3 indicated the existence of anatase and rutile phases of TiO₂ in all catalysts. The percentages of anatase and rutile phases were approximately 81 and 19%, while the crystallite sizes were approximately 21 and 81 nm, respectively. The characteristic peak of Mg was not detected due to it being present in trace amounts. In the FE-SEM images (Fig. S4), chlorophyll-modified catalysts (Fig. S4c and e) exhibited slightly larger size of agglomerated nanoparticles from unmodified catalysts (Fig. S4a and d) due to the partial coverage of chlorophyll over the catalyst surface. With *Spirulina* loading (Fig. S4b), P25 catalyst partly covered the smooth surface of large non-porous *Spirulina* particle (SEM images and the corresponding EDS results of pure *Spirulina* are shown in Fig. S5). Good dispersion of Mg atoms was observed in the EDS mapping image of 0.5Chl-0.1Mg/P25 (Fig. S4f).

In Fig. S6A, each catalyst gives a type IV isotherm with hysteresis loop, indicating the presence of mesoporous structure [53]. As shown in Table 2, for the same chlorophyll *a* loading amount, 0.5Sp/P25 showed less specific surface area and total pore volume compared to those of 0.5Chl/P25 catalyst due to the addition of *Spirulina* particles that naturally contain large amounts of proteins and other component [56,57] (Fig. S5). This is in good agreement with the results of SEM analysis. Therefore, the higher activity of 0.5Chl/P25 from 0.5Sp/P25 was due to the direct contact between chlorophyll and P25. The presence of an excess amount of chlorophyll (1.0Chl/P25) resulted in significant decreases in specific surface area and total pore volume as excess chlorophyll possibly

Table 2

Specific surface area, total pore volume, average pore size, and band gap of P25 and modified P25 catalysts.

Catalysts	Specific surface area (m^2/g)	Total pore volume (cm^3/g)	Average Pore size (nm)	Band gap (eV)
P25	57	0.57	40.2	3.02
0.5Sp/P25	19	0.42	86.6	2.82
0.1Chl/P25	52	0.74	56.8	2.87
0.5Chl/P25	36	0.65	72.3	2.82
1.0Chl/P25	19	0.36	75.0	2.43
0.1Mg/P25	56	0.57	40.6	2.92
0.5Chl-0.01Mg/P25	31	0.34	43.8	2.66
0.5Chl-0.1Mg/P25	24	0.35	58.8	2.60
0.5Chl-0.2Mg/P25	34	0.39	45.6	2.71

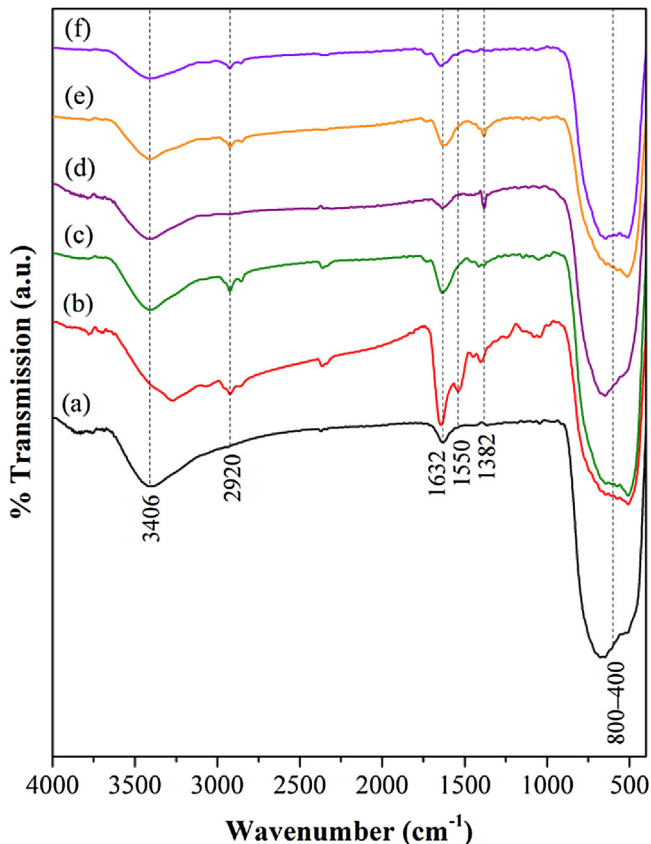


Fig. 3. FT-IR spectra of (a) P25, (b) 0.5Sp/P25, (c) 0.5Chl/P25, (d) 0.1Mg/P25, (e) 0.5Chl-0.1Mg/P25, and (f) 0.5Chl-0.2Mg/P25 (used) catalysts.

covered active sites of the P25 surface, resulting in a decrease in the photodegradation activity. Regarding the chlorophyll and Mg co-modified catalysts, as the physical properties of 0.1Mg/P25 were similar to those of P25 catalyst, loading chlorophyll on 0.1Mg/P25 (0.5Chl-0.1Mg/P25) resulted in a reduction in pore volume and pore size compared to those of chlorophyll-loaded P25 (0.5Chl/P25). These results indicated that chlorophyll and loaded Mg likely form a new complex structure during the loading process, leading to a synergistic effect between free Mg and chlorophyll. Moreover, the highest photocatalytic activity, attained with 0.5Chl-0.1Mg/P25, can also be attributed to the catalyst having the highest average pore size among all Chl-Mg/P25 catalysts.

FTIR spectra (Fig. 3) of all catalysts showed features attributed to TiO_2 around 3406, 1632, and 800–400 cm^{-1} , which originated from O–H stretching, O–H bending mode of $\text{Ti}–\text{OH}$, and O–Ti–O stretching adsorption band, respectively. The 0.5Sp/P25, 0.5Chl/P25, and 0.5Chl-0.1Mg/P25 catalysts (Fig. 3b, c, and e) displayed the presence of chlorophyll through the peaks associated with CH stretching of methyl, methylene or methine group at 2920 cm^{-1} , C=O stretching

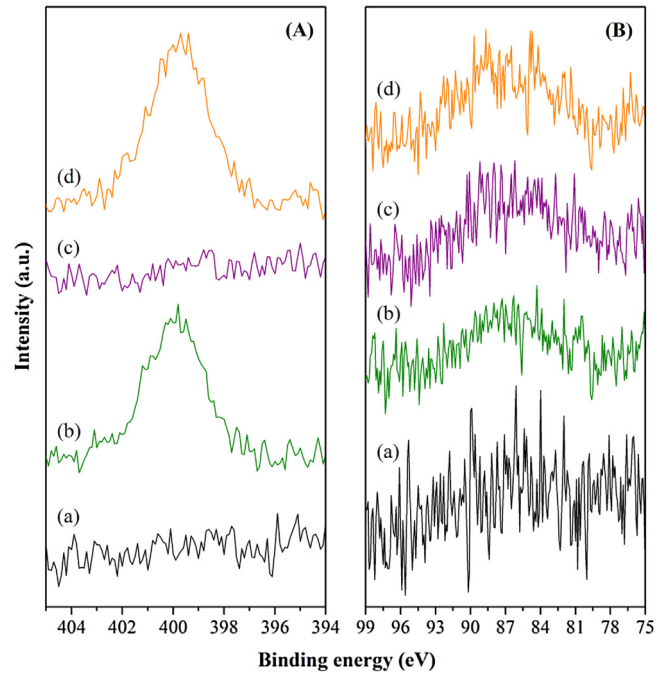


Fig. 4. High resolution XPS spectra of (A) N 1s and (B) Mg 2s of (a) P25, (b) 0.5Chl/P25, (c) 0.1Mg/P25, and (d) 0.5Chl-0.1Mg/P25 catalysts.

in conjugated ketone and carbonyl groups at 1632 cm^{-1} , and C=N stretching in chlorophyll around 1550 cm^{-1} [58,59], which were similar to the *Spirulina* spectrum in Fig. S7. In contrast to the P25 spectrum (Fig. 3a), the peak corresponding to NO_3^- ion asymmetric stretching (ν_3) mode at 1382 cm^{-1} was found in 0.1Mg/P25 and 0.5Chl-0.1Mg/P25 catalysts (Fig. 3d and e) [60,61], which indicated that NO_3^- ion incorporated on the catalyst surface.

3.3. Electronic state and coordination environments of metal atoms affecting the photodegradation activity of modified P25 catalysts

To examine the electronic properties of elements in the catalysts, an XPS study of P25 and modified P25 catalysts was carried out. High-resolution spectra of the N 1s of the catalysts are shown in Fig. 4A. The 0.5Chl/P25 and 0.5Chl-0.1Mg/P25 catalysts exhibited the N 1 s peak at 399.9 and 399.8 eV, respectively, representing the characteristics of nitrogen atoms in the porphyrin ring of chlorophyll [62], or a demetallation of chlorophyll caused by its exposure to X-rays during the experiment (which is a general feature of magnesium porphyrins [63,64]), while P25 and 0.1Mg/P25 catalysts did not show this peak. The XPS spectra of Mg 2 s shown in Fig. 4B exhibited a broad peak in 0.5Chl/P25, 0.1Mg/P25, and 0.5Chl-0.1Mg/P25 catalysts at approximately 86.5, 86.9, and 87.2 eV, respectively. The

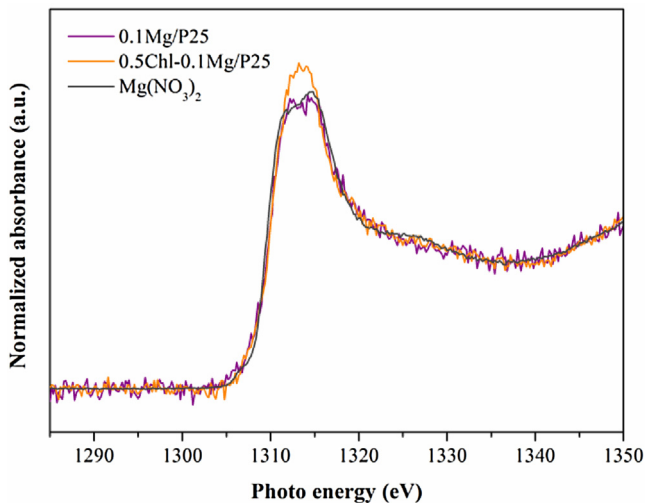


Fig. 5. Normalized Mg K-edge XANES spectra of 0.1Mg/P25, 0.5Chl-0.1Mg/P25 catalysts, and reference compound Mg(NO₃)₂.

Mg 2s peak centered at ~86.5–87.2 eV is attributed to the existence of Mg in the Mg²⁺ form on the catalyst surface [65].

The amounts of each element were calculated by weighting the areas of Ti 2p, O 1s, C 1s, N 1s, and Mg 2s photoemission peaks by the atomic sensitivity factors of each atomic level. It was found that the amount of magnesium in 0.5Chl-0.1Mg/P25 was approximately 2.72 at.%, which is almost equal to the sum of the amount of magnesium in 0.5Chl/P25 (1.82 at.%) and 0.1Mg/P25 catalysts (1.23 at.%) combined. This result evidently confirmed the presence of magnesium from both free Mg and chlorophyll-derived Mg loading on the 0.5Chl-0.1Mg/P25 catalyst.

XAS measurements were recorded at Mg K-edge to clearly confirm the local structure and electronic states of Mg in the catalysts. From Mg XANES spectra shown in Fig. 5 and Fig. S8, it can be seen that the oxidation state of Mg in 0.1Mg/P25, 0.5Chl/P25, and 0.5Chl-0.1Mg/P25 was Mg²⁺, which was in good agreement with the XPS results. The free-Mg loading was found to remain in Mg(NO₃)₂ phase after drying by microwave, as it exhibited similar features to standard Mg(NO₃)₂. Interestingly, increased white line intensity was observed for 0.5Chl-0.1Mg/P25 spectrum relative to 0.1Mg/P25 and 0.5Chl/P25 spectra, indicating a reduction in the 4p state population as the white line intensity depends on the density of electronic states [66]. These results confirmed that free Mg bonded with chlorophyll and formed a complex structure with a less filling state of Mg, resulting in the observed improvements of dye adsorption and photodegradation activity of Chl-Mg/P25 catalysts.

3.4. Improvement of visible-light absorption via surface modification of P25 catalysts

P25 was modified by magnesium and chlorophyll in order to enhance the visible-light absorption since the photocatalytic reaction rate is related to number of photons absorbed by the catalyst [5]. The absorption bands of modified P25 catalysts (Fig. 6b–i) revealed a red shift when compared with that of the P25 catalyst (Fig. 6a) and exhibited only the absorption in UV region at the absorption edge around 400 nm. This indicated a decrease in band gap energies of the modified P25 catalysts compared to unmodified P25 catalyst as shown in Table 2 (determined from the Kubelka–Munk plot in Fig. S9). With *Spirulina* and chlorophyll loadings (Fig. 6b–d), the visible-light absorptions in the region of 400–800 nm were improved. This was mainly caused by the existence of chlorophyll a, as was confirmed by the similar absorption

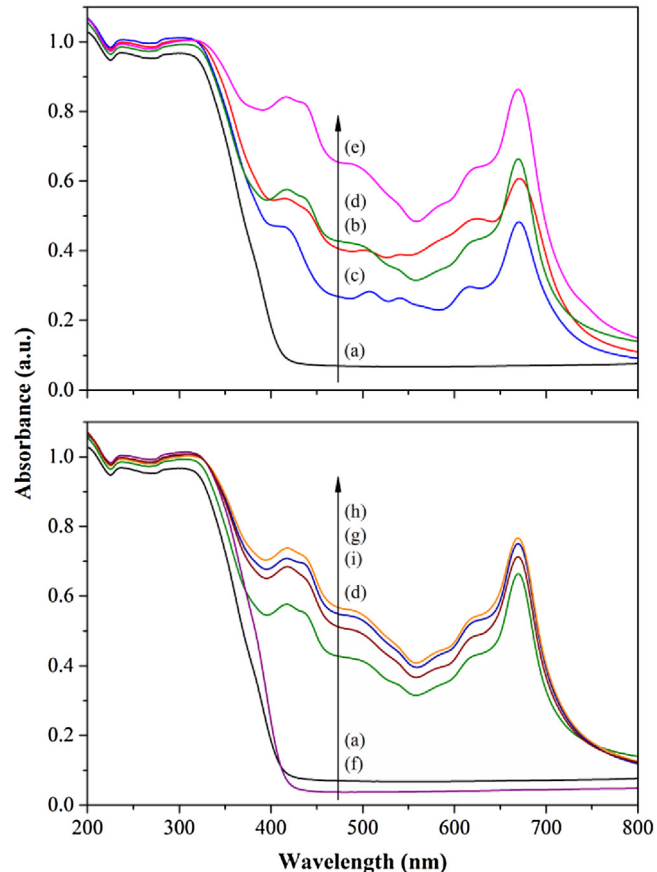


Fig. 6. UV-vis diffuse reflectance spectra of P25 and modified P25 catalysts: (a) P25, (b) 0.5Sp/P25, (c) 0.1Chl/P25, (d) 0.5Chl/P25, (e) 1.0Chl/P25, (f) 0.1Mg/P25, (g) 0.5Chl-0.01Mg/P25, (h) 0.5Chl-0.1Mg/P25, and (i) 0.5Chl-0.2Mg/P25 catalysts.

capacities of 0.5Sp/P25 and 0.5Chl/P25 (absorption spectra of *Spirulina* and extracted chlorophyll are shown in Fig. S10).

In the case of free-Mg loading, the presence of free Mg on P25 (Fig. 6f) led to lower visible-light absorption (Fig. 6a). However, as it can be seen in Fig. 2B, 0.1Mg/P25 catalyst showed a slightly higher photodegradation efficiency than that of P25 catalyst despite the lower visible-light absorption and similar physical properties to those of P25 catalyst (Table 1). This implied that free Mg in Mg²⁺ form acts as electron-trapping sites and helps inhibit the recombination of electron-hole pairs, resulting in an enhancement of the photoactivity. There have also been few literature [67–69] proposed that Mg²⁺ can trap photo-generated electrons and hence improve the photocatalytic activity. On the other hand, adding free Mg onto the chlorophyll (bound-Mg) modified P25 catalysts (Fig. 6g–i) exhibited the opposite result to the free-Mg-modified catalyst by significantly enhancing the visible-light absorption capacity of the catalyst (Fig. 6d). With 0.5Chl-0.1Mg/P25 catalyst the absorption capacity was considerably enhanced. These findings indicated a synergistic effect of the presence of free Mg together with chlorophyll in the improvement of the visible-light absorption. Among all catalysts, 0.5Chl-0.1Mg/P25 exhibited the highest visible-light absorption with the lowest

3.5. Charge and energy transfer between P25 catalyst, chlorophyll, and Mg

To investigate the charge transfer and recombination of electron-hole pairs in the photocatalysts, PL spectroscopy was performed over P25 and modified P25 catalysts at an excitation wavelength of 255 nm (Fig. 7). All the catalysts displayed a sim-

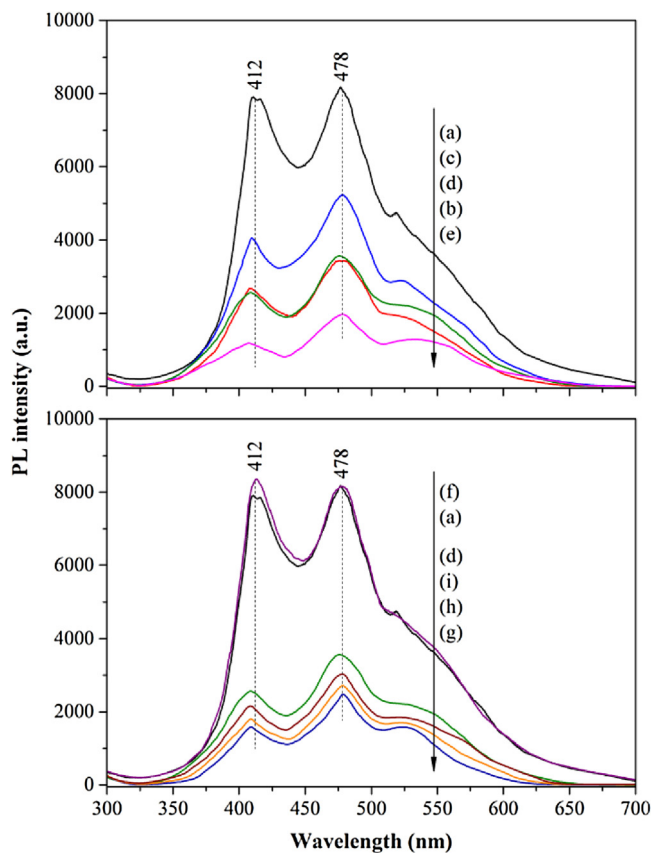


Fig. 7. PL spectra of P25 and modified P25 catalysts: (a) P25, (b) 0.5Sp/P25, (c) 0.1Chl/P25, (d) 0.5Chl/P25, (e) 1.0Chl/P25, (f) 0.1Mg/P25, (g) 0.5Chl-0.01Mg/P25, (h) 0.5Chl-0.1Mg/P25, and (i) 0.5Chl-0.2Mg/P25 catalysts (excitation at 255 nm).

ilar curve shape mainly consisting of two strong emission peaks centered at approximately 412 and 478 nm. Compared with P25 catalyst, proportional decreases in PL intensities of Chl/P25 catalysts were observed, indicating a charge transfer between P25 catalyst and chlorophyll [35]. In addition, *Spirulina* also significantly lowered the PL intensity of P25 catalyst (0.5Sp/P25) to nearly the same extent as 0.5Chl/P25 catalyst. This result evidently implied that chlorophyll in *Spirulina* is the key factor in lowering the PL intensity, leading to an improvement of photoactivity. The energy levels, reported by Kathiravan et al. [70], indicated electron transfer direction from chlorophyll excited states to the catalyst conduction band; similar direction of charge transfer has also been reported in other works [37,38,71], wherein a higher oxidation potential of chlorophyll at excited states (−1.27 vs. SCE) compared to that of TiO₂ conduction band (−0.1 vs. SCE) was also observed. Chlorophyll in *Spirulina* could potentially act as a photosensitizer or electron donor; as a result, these additional electrons from chlorophyll help facilitate the photocatalytic reaction by participating in the degradation process of adsorbed dye molecules on the catalyst surface. However, the large population of photo-induced electron-hole pairs resulting from a high chlorophyll loading amount (1.0 wt.%) had a negative result as they promoted the formation of recombination centers and inhibited the interfacial electron-hole transfer, leading to a decrease of photocatalytic activity under visible light [72–74].

It should be noted that the free-Mg-loaded P25 catalyst, 0.1Mg/P25, exhibited an almost similar PL intensity to that of P25 catalyst. In contrast, the PL intensities of free Mg loaded on 0.5Chl/P25 catalyst were proportionally decreased with the decrease of Mg loading. As it is known that PL emission represents the recombination of free-charge carriers [5,75,76], the decrease

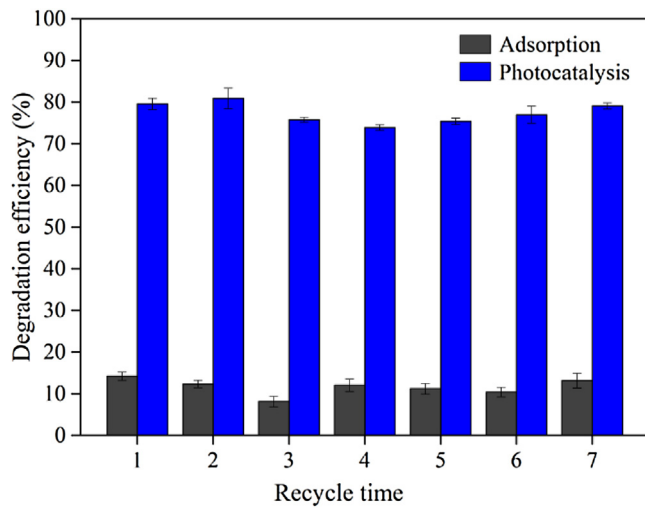


Fig. 8. Cycling run for the photocatalytic degradation of rhodamine B over 0.5Chl-0.1Mg/P25 catalyst.

in PL intensities of Chl-Mg/P25 catalysts indicates the outstanding inhibition of the recombination of photo-induced electron-hole pairs and higher charge separation efficiency, as a result of the synergistic effect caused by the presence of chlorophyll together with free Mg, as was previously mentioned when discussing the results pertaining to the visible-absorption capacity of co-modified Chl-Mg/P25 catalysts. In addition, the decrease in PL intensity of Chl-Mg/P25 catalysts also indicated that the small amount of Mg could better inhibit the recombination of photo-induced electron-hole pairs than high amount of Mg due to the fact that the excess amount of Mg could turn into charge recombination centers. However, in the case of 0.1Mg/P25, almost similar PL intensity to that of P25 catalyst was observed, this might be due to the small effect of high loading amount of Mg.

3.6. Recyclability of Chl-Mg/P25 catalyst

The reusability and photostability of catalysts are among the most important factors in the practical applications of industrial catalysts. To investigate these properties, the catalyst with the highest photodegradation activity of RhB under visible light irradiation (0.5Chl-0.1Mg/P25) was examined for recycling performance. After each run, the photocatalyst was collected by simple filtration and dried at 60 °C for 12 h before performing the repeated experiments under similar conditions as described in the experimental section. As shown in Fig. 8, the dye adsorption and photocatalytic degradation efficiencies of 0.5Chl-0.1Mg/P25 catalyst remained nearly unchanged, and a photocatalytic efficiency of more than 75% was achieved after seven repeated experiments. These results evidently indicated the good recyclability and high stability of 0.5Chl-0.1Mg/P25 catalyst.

FT-IR analysis of the used 0.5Chl-0.1Mg/P25 catalyst (Fig. 3f) was performed and compared to that of fresh catalyst (Fig. 3e). The peak intensity at 1382 cm⁻¹ (corresponding to NO₃⁻ ion) of the used catalyst after a seven-cycle photocatalytic experiment disappeared due to the fact that NO₃⁻ ion dissolved into the dye solution. However, as the photocatalytic activity of the catalyst saw almost no change, it can be concluded that NO₃⁻ ion was therefore not responsible for the enhancement in the photocatalytic performance. The remaining chlorophyll in the used catalyst based on a peak at 2920 cm⁻¹ (CH stretching of methyl, methylene or methine group in chlorophyll) which only appeared in chlorophyll-loaded catalysts was found to be approximately 88%. This indicated a good stability of chlorophyll in a form of complex Chl-Mg struc-

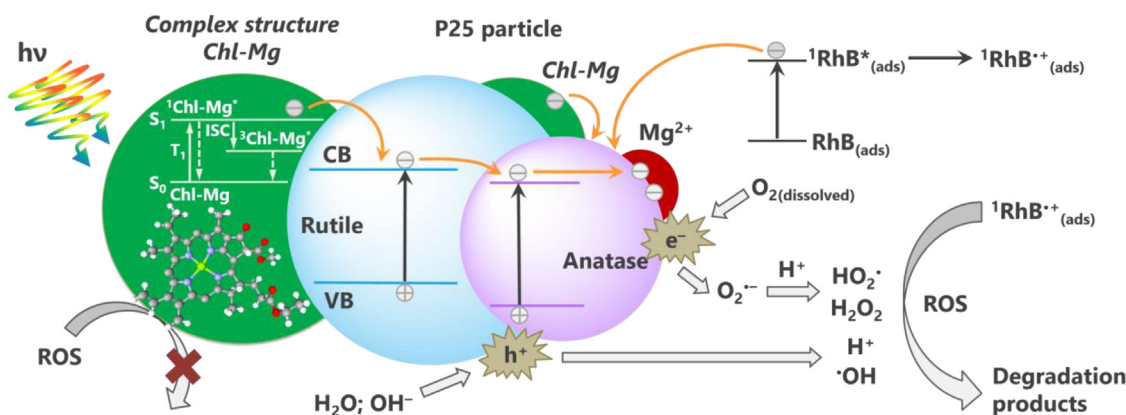


Fig. 9. Proposed mechanism for photocatalytic degradation of RhB on chlorophyll-Mg co-modified P25 catalyst.

ture in Chl-Mg/P25 catalysts. The addition of Mg^{2+} in form of $MgCl_2$ or $Mg(NO_3)_2$ in chlorophyll solution was also reported to inhibit chlorophyll degradation as well [77,78].

In order to further evaluate the photostability of Chl-Mg/P25 catalysts, the fresh 0.5Chl-0.1Mg/P25 catalyst, and used catalyst as well as a residual solution after RhB completely degraded ($C=0$) were analyzed by using ICP-OES. The amount of Mg in the fresh catalyst was 0.075% (w/w), while the remaining Mg left in the used catalyst and Mg ion in a residual solution were found to be 0.054% (w/w) and 0.0141 mg (0.47 mg/L), respectively. This indicated that approximately 28% of unstable Mg in the catalyst was dissolved into the solution. From all the preceding results, it can be summarized that the complex structure between free Mg and chlorophyll is likely the key parameter which controls the mechanism and remarkably increases photocatalytic performance and stability. Accordingly, 0.5Chl-0.1Mg/P25 catalyst is a promising candidate for photocatalytic applications due to its high photocatalytic efficiency, reusability, and stability, along with low energy consumption.

3.7. Proposed reaction mechanism over Chl-Mg/P25 catalyst

In the photocatalytic degradation and recyclability results, co-modified P25 catalyst with chlorophyll and Mg has enhanced the catalyst activity compared to un-modified P25 and single-modified P25 catalyst due to a synergistic effect between chlorophyll and free Mg on the mixed-phase TiO_2 catalyst. A schematic illustration of the proposed reaction mechanism with the charge separation and transfer of photocatalytic degradation of RhB is given in Fig. 9.

Under visible light irradiation, RhB as a dye-sensitized material absorbs visible light photons and promotes electrons from a ground state to an excited state in the organic molecules. At the same time, a new stable form of free Mg bonded with chlorophyll (Chl-Mg) as the surface complex, that can be attached to both anatase and rutile phases of P25, also absorbs photons and excites electrons to an excited singlet state ($^1\text{Chl-Mg}^*$), and some electrons undergo intersystem crossing (ISC) to their triplet state ($^3\text{Chl-Mg}^*$). The electrons can then transfer from both RhB and the Chl-Mg excited state to the P25 conduction band (CB), leading to the formation of RhB \cdot^+ molecular ion radicals and a cationic form of chlorophyll-Mg (Chl-Mg $^+$) on the P25 surface. Moreover, P25 can create electron-hole pairs by absorbing some photons with energy equal to or higher than band gap energy (E_g).

The electrons in the P25 conduction band then react with adsorbed oxygen on the P25 surface to produce superoxide radical ($O_2\cdot^-$), while holes in P25 valence band (VB) react with the surface water or hydroxyl group to produce reactive oxygen species (ROS), such as hydroxyl radical ($\cdot OH$), hydroperoxyl radical ($HO_2\cdot$), and

hydrogen peroxide (H_2O_2). After that, these highly-reactive radical species react with RhB molecules, leading to the completion of the degradation cycle of the RhB. In addition, the remaining free Mg in the Mg^{2+} form on the P25 surface can trap the excited electrons and prevent the recombination of electron-hole pairs, allowing more free charges to participate in the degradation reactions. The complex Chl-Mg structures moreover inhibit the binding between ROS and nitrogen sites in porphyrin ring of chlorophyll, which is known to initiate the chlorophyll degradation [79–81]; accordingly the better photodegradation performance and good reusability of catalysts are evidently observed.

4. Conclusion

Unique chlorophyll and Mg co-modified P25 (Chl-Mg/P25) catalyst was prepared, and the improvement it can provide in catalytic performance of RhB photodegradation was examined. Under visible light irradiation, the activities of catalysts were found to be in the order of: P25 < Mg/P25 < Sp/P25 < Chl/P25 < Chl-Mg/P25. The high activity of Chl/P25 could be attributed to the role of chlorophyll that acted as a photosensitizer and donated electrons to P25 conduction bands and the direct contact between chlorophyll and P25. More importantly, the further enhancement of photocatalytic activity of Chl-Mg/P25 from single-modified catalysts was likely due to the formation of a complex structure between free Mg and chlorophyll, as confirmed by XANES analysis. This new complex Chl-Mg structure causes significant increases in visible-light absorption and dye adsorption capacities, as well as improves the reusability of the catalysts. The outstanding performance of Chl-Mg/P25 catalysts can also be attributed to the remaining free Mg in the Mg^{2+} form that acted as a trapping site of the charges carrier and effectively separated photo-induced electron and holes, as shown in the PL results. Accordingly, free Mg and chlorophyll together play a key role in the improvement of the performance of Chl-Mg/P25 catalyst. However, high percentages of chlorophyll and free Mg could inversely turn to recombination centers and decrease the degradation efficiency as well.

Acknowledgements

This work was financially supported by grants from the Thailand Research Fund through the Royal Golden Jubilee Ph.D. Program (Grant No. PHD/0074/2554), the Center for Advanced Studies in Nanotechnology for Chemical, Food and Agricultural Industries, and the Kasetsart University Research and Development Institute (KURDI).

Appendix A. Supplementary data

Supplementary data associated with this article can be found, in the online version, at <http://dx.doi.org/10.1016/j.apcatb.2017.02.042>.

References

- [1] T.R. Cook, D.K. Dogutan, S.Y. Reece, Y. Surendranath, T.S. Teets, D.G. Nocera, Chem. Rev. 110 (2010) 6474–6502.
- [2] G.A. Olah, A. Goeppert, G.K.S. Prakash, J. Org. Chem. 74 (2009) 487–498.
- [3] K. Nakata, A. Fujishima, J. Photochem. Photobiol. C 3 (2012) 169–189.
- [4] M. Ni, M.K.H. Leung, D.Y.C. Leung, K. Sumathy, Renew. Sustain. Energy Rev. 11 (2007) 401–425.
- [5] H. Xu, J. Yan, Y. Xu, Y. Song, H. Li, J. Xia, C. Huang, H. Wan, Appl. Catal. B 129 (2013) 182–193.
- [6] A. Zaleska, Recent Pat. Eng. 2 (2008) 157–164.
- [7] M. Kitano, M. Matsuoka, M. Ueshima, M. Anpo, Appl. Catal. A 325 (2007) 1–14.
- [8] L.-L. Tan, W.-J. Ong, S.-P. Chai, A.R. Mohamed, Appl. Catal. B 166–167 (2015) 251–259.
- [9] X. Yang, J. Qin, Y. Jiang, K. Chen, X. Yan, D. Zhang, R. Li, H. Tang, Appl. Catal. B 166–167 (2015) 231–240.
- [10] K. Li, T. Chen, L. Yan, Y. Dai, Z. Huang, H. Guo, L. Jiang, X. Gao, J. Xiong, D. Song, Catal. Commun. 28 (2012) 196–201.
- [11] J.L. White, M.F. Baruch, J.E. Pander III, Y. Hu, I.C. Fortmeyer, J.E. Park, T. Zhang, K. Liao, J. Gu, Y. Yan, T.W. Shaw, E. Abelev, A.B. Bocarsly, Chem. Rev. 115 (2015) 12888–12935.
- [12] J. Sun, L. Gao, Q. Zhang, J. Am. Ceram. Soc. 86 (2003) 1677–1682.
- [13] S.-J. Kim, H.-G. Lee, S.-J. Kim, J.-K. Lee, E.G. Lee, Appl. Catal. A 242 (2003) 89–99.
- [14] A.Y. Ahmed, T.A. Kandiell, T. Oekermann, D. Bahnemann, J. Phys. Chem. Lett. 2 (2011) 2461–2465.
- [15] C. Su, B.Y. Hong, C.M. Tseng, Catal. Today 96 (2004) 119–126.
- [16] T. Ohno, K. Sarukawa, K. Tokieda, M. Matsumura, J. Catal. 203 (2001) 82–86.
- [17] G.H. Li, S. Ciston, Z.V. Saponjic, L. Chen, N.M. Dimitrijevic, T. Rajh, K.A. Gray, J. Catal. 253 (2008) 105–110.
- [18] X. Sun, W. Dai, G. Wu, L. Li, N. Guanab, M. Hunger, Chem. Commun. 51 (2015) 13779–13782.
- [19] D.O. Scanlon, C.W. Dunnill, J. Buckeridge, S.A. Shevlin, A.J. Logsdail, S.M. Woodley, C.R.A. Catlow, M.J. Powell, R.G. Palgrave, I.P. Parkin, G.W. Watson, T.W. Keal, P. Sherwood, A. Walsh, A.A. Sokol, Nat. Mater. 12 (2013) 798–801.
- [20] Y. Mi, Y. Weng, Sci. Rep. 5 (2015) (ID 11482).
- [21] X. Wu, S. Yin, Q. Dong, T. Sato, Appl. Catal. B 156–157 (2014) 257–264.
- [22] C.Z. Wen, J.Z. Zhou, H.B. Jiang, Q.H. Hu, S.Z. Qiao, H.G. Yang, Chem. Commun. 47 (2011) 4400–4402.
- [23] G.K. Mor, O.K. Varghese, M. Paulose, K. Shankar, C.A. Grimes, Sol. Energy Mater. Sol. Cells 90 (2006) 2011–2075.
- [24] W.-J. Ong, L.-L. Tan, S.-P. Chai, S.-T. Yonga, A.R. Mohamed, Nanoscale 6 (2014) 1946–2008.
- [25] B. Ma, J. Guo, W.-L. Dai, K. Fan, Appl. Catal. B 130–131 (2013) 257–263.
- [26] S. Zhang, S. Zhang, L. Song, Appl. Catal. B 152–153 (2014) 129–139.
- [27] L. Chen, S. Yang, B. Hao, J. Ruan, P.-C. Ma, Appl. Catal. B 166–167 (2015) 287–294.
- [28] M. Kim, Y.K. Kim, S.K. Lim, S. Kim, S.-I. In, Appl. Catal. B 166–167 (2015) 423–431.
- [29] H.-C. Liang, X.-Z. Li, Appl. Catal. B 86 (2009) 8–17.
- [30] O. Rosseler, C. Ulhaq-Bouillet, A. Bonnefont, S. Pronkin, E. Savinova, A. Louvet, V. Keller, N. Keller, Appl. Catal. B 166–167 (2015) 381–392.
- [31] N. Shi, X. Li, T. Fan, H. Zhou, D. Zhang, H. Zhu, Int. J. Hydrot. Energy 39 (2014) 5617–5624.
- [32] S. Murata, H. Furukawa, K. Kuroda, Chem. Mater. 13 (2001) 2722–2729.
- [33] Y. Tomonou, Y. Amao, Int. J. Hydrot. Energy 29 (2004) 159–162.
- [34] M. Yoshimoto, T. Furuya, N. Kunihiro, Colloids Surf. A 387 (2011) 65–70.
- [35] H. Hagiwara, T. Inoue, K. Kaneko, T. Ishihara, Chem. Eur. J. 15 (2009) 12862–12870.
- [36] Y.-S. Lai, Y.H. Su, M.I. Lin, Dyes Pigm. 103 (2014) 76–81.
- [37] M. Joshi, S.P. Kamble, N.K. Labhsetwar, D.V. Parwate, S.S. Rayalu, J. Photochem. Photobiol. A 204 (2009) 83–89.
- [38] S. Benjamin, D. Vaya, P.B. Punjabi, S.C. Ameta, Arabian J. Chem. 4 (2011) 205–209.
- [39] C.-W. Lee, R.A. Kourounioti, J.C.S. Wu, E. Murchie, M. Maroto-Valer, O.E. Jensen, C.-W. Huang, A. Ruban, J. CO₂ Util. 5 (2014) 33–40.
- [40] T. Phongamwong, M. Chareonpanich, J. Limtrakul, Appl. Catal. B 168 (2015) 114–124.
- [41] E.D.G. Danesi, C.O. Rangel-Yagui, J.C.M. Carvalho, S. Sato, Biomass Bioenergy 26 (2004) 329–335.
- [42] O. Jorquera, A. Kiperstok, E.A. Sales, M. Embiruçu, M.L. Ghirardi, Bioresour. Technol. 101 (2010) 1406–1413.
- [43] S. Qin, F. Xin, Y. Liu, X. Yin, W. Ma, J. Colloid Interface Sci. 356 (2011) 257–261.
- [44] L. Xiang, X. Zhao, C. Shang, J. Yin, J. Colloid Interface Sci. 403 (2013) 22–28.
- [45] P. Pawinrat, O. Mekasuwandumrong, J. Panpranot, Catal. Commun. 10 (2009) 1380–1385.
- [46] J. Bandara, C.C. Hadapangoda, W.G. Jayasekera, Appl. Catal. B 50 (2004) 83–88.
- [47] S. Xie, Y. Wang, Q. Zhang, W. Fan, W. Deng, Y. Wang, Chem. Commun. 49 (2013) 2451–2453.
- [48] G.S. Han, H.S. Chung, B.J. Kim, D.H. Kim, J.W. Lee, B.S. Swain, K. Mahmood, J.S. Yoo, N.-G. Park, J.H. Lee, H.S. Jung, J. Mater. Chem. A 3 (2015) 9160–9164.
- [49] A. Bennett, L. Bogorad, J. Cell Biol. 58 (1973) 419–435.
- [50] R.A.R. Monteiro, S.M. Miranda, V.J.P. Vilar, L.M. Pastrana-Martínez, P.B. Tavares, R.A.R. Boaventura, J.L. Faria, E. Pinto, A.M.T. Silva, Appl. Catal. B 162 (2015) 66–74.
- [51] D. Li, Q. Zhu, C. Han, Y. Yang, W. Jiang, Z. Zhang, J. Hazard. Mater. 285 (2015) 398–408.
- [52] M. El-Kemary, H. El-Shamy, I. El-Mehasseb, J. Lumin. 130 (2010) 2327–2331.
- [53] K. Natarajan, T.S. Natarajan, H.C. Bajaj, R.J. Tayade, Chem. Eng. J. 178 (2011) 40–49.
- [54] J. Di, J. Xia, Y. Ge, H. Li, H. Ji, H. Xu, Q. Zhang, H. Li, M. Li, Appl. Catal. B 168–169 (2015) 51–61.
- [55] D. Li, H. Zheng, Q. Wang, X. Wang, W. Jiang, Z. Zhang, Y. Yang, Sep. Purif. Technol. 123 (2014) 130–138.
- [56] A.S. Gad, Y.A. Khadraby, A.A. El-Nekeety, S.R. Mohamed, N.S. Hassan, M.A. Abdel-Wahhab, Nutrition 27 (2011) 582–589.
- [57] R.E. Avendaño-Herrera, C.E. Riquelme, Aquacult. Eng. 36 (2007) 97–104.
- [58] F. Xu, Q.-A. Zhou, J.-X. Sun, C.-F. Liu, J.-L. Ren, R.-C. Sun, S. Curling, P. Fowler, M.S. Baird, Process Biochem. 42 (2007) 913–918.
- [59] Z. Mehraban, F. Farzaneh, A. Shafeikhani, Opt. Mater. 29 (2007) 927–931.
- [60] M. Sulaiman, A.A. Rahman, N.S. Mohamed, Int. J. Electrochem. Sci. 8 (2013) 6647–6655.
- [61] G. Zou, R. Liu, W. Chen, Mater. Lett. 61 (2007) 1990–1993.
- [62] S. Muralidharan, R.G. Hayes, J. Am. Chem. Soc. 102 (1980) 5106–5107.
- [63] D.H. Karweik, N. Winograd, Inorg. Chem. 15 (1976) 2336–2342.
- [64] G. Polzonetti, C. Battocchio, A. Goldoni, R. Larciprete, V. Carravetta, R. Paolesse, M.V. Russo, Chem. Phys. 297 (2004) 307–314.
- [65] Y. Luo, X. Wang, W. Guo, M. Rohwerder, J. Electrochem. Soc. 162 (2015) C294–C301.
- [66] A. Halder, Q. Jia, M. Trahan, S. Mukerjee, Electrochim. Acta 108 (2013) 288–295.
- [67] X. Xue, W. Ji, Z. Mao, C. Zhao, B. Zhao, J.R. Lombardi, RSC Adv. 3 (2013) 20891–20895.
- [68] H. Nouri, A. Habibi-Yangjeh, Adv. Powder Technol. 25 (2014) 1016–1025.
- [69] T.S. Rao, T.A. Segne, T. Susmitha, A.B. Kiran, C. Subrahmanyam, Adv. Mater. Sci. Eng. (2012) 2012 (ID 168780).
- [70] A. Kathiravan, M. Chandramohan, R. Renganathan, S. Sekar, Spectrochim. Acta Part A 71 (2009) 1783–1787.
- [71] Y. Saiki, Y. Amao, Int. J. Hydrot. Energy 29 (2004) 695–699.
- [72] D. Pei, J. Luan, Int. J. Photoenergy (2012) 2012 (ID 262831).
- [73] I. Tseng, J.C.-S. Wu, Catal. Today 97 (2004) 113–119.
- [74] X. Li, Z. Zhuang, W. Li, H. Pan, Appl. Catal. A 429–430 (2012) 31–38.
- [75] S. Sun, J. Ding, J. Bao, C. Gao, Z. Qi, X. Yang, B. He, C. Li, Appl. Surf. Sci. 258 (2012) 5031–5037.
- [76] P. Pawinrat, O. Mekasuwandumrong, J. Panpranot, Catal. Commun. 10 (2009) 1380–1385.
- [77] F. Vicentini, F. Iten, P. Matile, Physiol. Plant. 94 (1995) 57–63.
- [78] M.L. Costa, P.M. Civello, A.R. Chaves, G.A. Martínez, Plant Physiol. Biochem. 40 (2002) 111–118.
- [79] T. Kunieda, T. Amano, Y. Shioi, Plant Sci. 169 (2005) 177–183.
- [80] K. Takamiya, T. Tsuchiya, H. Ohta, Trends Plant Sci. Rev. 5 (2000) 426–431.
- [81] S. Barazzouk, L. Bekalé, S. Hotchandani, J. Mater. Chem. 22 (2012) 25316–25324.